TUDelft

Delft University of Technology

Dynamic coherence scanning interferometry based on an optical phase mask for simultaneous measurement of local induced vibration and local topology change of a mirror

Vilaboa Pérez, Jesús; Georges, Marc; Hastanin, Juriy ; Loicq, J.J.D.

Dynamic coherence scanning interferometry based on an optical phase mask for simultaneous measurement of local induced vibration and local topology change of a mirror

Jesús Vilaboa Pérez◉,a,* **Marc Georges**◉,a **Juriy Hastanin,**a **and Jérôme Loicq**a,b

aUniversité de Liège, STAR Institute, Centre Spatial de Liège, Liège, Belgium
bDelft University of Technology, Faculty of Aerospace Engineering, Delft, The Netherlands

ABSTRACT. We describe the state of the development of a coherence scanning interferometer to measure local changes in topology and local induced vibrations of a mirror at cryogenic temperatures. The metrology instrument incorporates an optical phase mask and a microlenses array, enabling the acquisition of complete white light interferograms within a single-camera frame. This stands in contrast to traditional temporal phase-shifting interferometers. We design the optical phase mask as a combination of steps of different thicknesses, so each step introduces a different optical path difference to the rays. The local interferograms for each camera frame provide us with information on the local topology of the mirror. The interferogram displacement between camera frames allows us to monitor the mirror's local induced vibrations. In this work, we report the metrology instrument's working principle through numerical simulations and present the latest results of a proof of concept developed at the laboratory. The metrology instrument shown is of extensive usability in diverse applications related to real-time measurements of various fast physical processes and real-time characterization of the optical components topology.

© 2024 Society of Photo-Optical Instrumentation Engineers (SPIE) [DOI: 10.1117/1.OE.63.2.024111]

Keywords: coherence scanning interferometry; dynamical interferometry; optical phase mask; single-frame low-coherence interferometry; topology characterization; induced vibrations characterization

1 Introduction

Coherence scanning interferometry (CSI), also known as white-light interferometry, is widely used for characterizing the topography of optical components.[1] A well-differentiated central fringe describes the interference pattern obtained with a low-coherence source. This zero-order fringe is visible only within the limits of the source coherence length.[2,3] As a result, with a white light interferogram, it is possible to determine the value of local topography unambiguously. In addition, with a low-coherence source, we avoid the 2π ambiguity in conventional high-coherence sources. Moreover, the short coherence of the source is an advantage in avoiding spurious unwanted interferometry signals from scattered rays, speckle, dust, and imperfections.[4] Most commonly, CSI is used for surface topography measurements. However, it is also employed for out-of-plane vibration measurements, e.g., as shown by De Groot[5] with a stroboscopic coherence scanning interferometer to measure kHz out-of-plane vibrations.

---

*Address all correspondence to Jesús Vilaboa Pérez, jvilaboaperez@uliege.be

In this paper, we present the conceptual design, numerical simulation results and a proof of concept of a coherence scanning interferometer that simultaneously measures local induced vibrations and local topology changes. We aim to confirm the measurement principle of the instrument. The interferometer under development involves a low-coherence source of at least 200 nm bandpass in the visible region of the electromagnetic spectrum ranging between 500 and 700 nm. The presented metrology instrument includes a microlenses array and an optical phase mask to perform dynamic single-frame interferometry. The aim of the microlenses array is to obtain a repetition of the interference pattern of the mirror surface under characterization on a single-camera frame. The optical phase mask is used to introduce a different phase shift for each of the interference patterns. The interference patterns are linked to the local topology of the mirror under test. Accordingly, we can determine local induced out-of-plane low-frequency vibrations by analyzing the interference patterns of consecutive camera frames. Our work addresses the frequency range of induced vibration of the mirror from 0.1 to 10 Hz.

The concept of dynamical interferometry has been the object of several studies as a method to perform fast measurements and avoid unwanted mechanical vibrations. It contrasts with the traditional interferometry methods that require multiple camera frames and a translation stage to reconstruct the interference patterns (i.e., temporal phase-shifting). Heterodyne interferometry is a well-known technique used to obtain optical phase information on a single-shot measurement and measure mirror displacements. This method involves superposing two laser beams with slightly different frequencies to produce a heterodyne signal, which is used to accurately measure changes in length.[6] Millerd and North-Morris summarized other advanced techniques for dynamic interferometry.[7] One of the main methods uses a micro-polarizer phase shifting array aligned to a detector array. This approach makes obtaining four phase-shifted interferograms on a single camera frame possible. The light source used for this instantaneous phase-shifting inter-ferometer is a single-mode laser. Kwon presents the technique for performing instantaneous laser phase-shifting using pinholes on grating substrates.[8] In addition, Pavliček et al. recently presented a metrology instrument based on white light interferometry that uses a built-in fiber stretcher to change the optical path difference (OPD) without mechanical scanning components.[9] The fiber stretcher modulates the white light source spectrum and modifies its spectral period for the scanning process. Takeda describes a single-shot broadband source technique for film-thickness measurements.[6] This technique uses a Wollaston prism to compensate for the time delay between the beams reflected from the top and bottom surfaces of the film, which is proportional to the film thickness. Moreover, Ferrec et al. presented the concept of a phase mask for interferometry based on a set of Fabry–Perot interferometers of different cavity widths.[10] Therefore, with a dynamic interferometer, we can perform fast measurements of the optical component's topology and avoid unwanted external disturbances between camera frames. With our metrology instrument, we aim to obtain more than 25 phase-shifted interference patterns on a single camera frame to reduce the effect of the noise on the measurements.

In addition to the interferogram data acquisition, another challenging issue is determining the peak of the coherence envelope that wraps the zero-order fringe. In general, there are two main groups of methods for this peak detection. The first group looks directly for the highest point of the envelope, like the well-known centroid method.[11] The second group is a more sensitive approach that uses the white-light interference phase,[2] highlighting the phase shifting interferometry (PSI) method and techniques performing a Fourier analysis of the interference data.[2,3] It is instructive to note that a phase shift is introduced not only by changing the optical path of the rays but also by a cyclic change in the polarization of the light beam.[12] For our instrument, we select the method that adapts the best to the optical phase mask designed. We also worked on new approaches and data processing methods to adapt to the prototype of the optical phase mask built.

Finally, we present the results of the experimental investigations on the first proof of concept of the proposed metrology instrument. We explain how we obtain the interference fringes and validate the proposed white light interferometry approach involving a microlenses array.

We develop the proposed metrology instrument for the E-TEST technology demonstrator of the future Einstein Telescope (ET). ET is an interferometric gravitational wave observatory aiming to detect gravitational waves (GWs) with a sensitivity a thousand times better than the previous generation. The E-TEST demonstrator aims to prove the improvement in the stability of the GW mirror used in the ET interferometer under cryogenic temperature.[13–16] During the

cooling down phase, the mirror may be affected by surface topology changes due to mechanical stress and induced vibrations. Kaneda et al. showed the topology change of a large mirror working at cryogenic temperatures.[17] Hence, our instrument's mirror characterization is essential for the accuracy of results in detecting GWs.

Several references address the characterization of large mirrors at cryogenic temperatures. Kaneda et al. used a mechanical phase-shifting laser interferometer to test the cryogenic performance of carbon-fiber-reinforced silicon carbide (C/SiC) mirror.[17] Another example is the surface deformation test of the James Webb Space Telescope mirrors. The test was conducted in a high-vibration environment at cryogenic temperature. To maintain vibration insensitivity, a dynamic laser interferometer equipped with a pixelated-polarized mask was used to conduct the measurements.[18] In the E-TEST project, we add the challenge of characterizing the mirror while it is suspended by a hanging module inside the vacuum chamber for stabilization purposes.

The instrument is also useful for inspecting the surface topography of other optical components. Thanks to the inherent dynamical aspects of the proposed approach, we can use it for fast characterizations with all the cited advantages of CSI.

2 Methods

2.1 Definition of the White Light Interference Pattern

We can assume that the white light source shape of the bandpass is a Gaussian. In that case, we can define the interference pattern as the combination of the normal probability density function and the fundamental equation of interferometry,[19–21] obtaining the following equation:

$$I(\mathrm{OPD}) = 0.5 \cdot I_0 \cdot \left(1 + \exp\left[-\left(\frac{\mathrm{OPD}}{l_c}\right)^2\right]\right) \cdot \cos(2 \cdot k_0 \cdot \mathrm{OPD}), \quad (1)$$

where k_0 is the wavenumber ($k_0 = 2\,\pi/\lambda$), λ is the central wavelength of the source, and l_c is the coherence length defined in Eq. (2).[4] The coherence length is the distance the wave travels before the temporal coherence drops to zero. As a result, the peak of the white light interference pattern is only visible if the OPD between the interferometer's two arms is less than half the source coherence length. The white light pattern has a periodic modulation with a period of $\lambda/2$

$$lc = \sqrt{\frac{2\ln(2)}{\pi n}} \frac{\lambda_0^2}{\mathrm{FWHM}(\lambda)}, \quad (2)$$

where FWHM is the full wave half maximum defined at the 1/e of the highest point of the coherence envelope, n is the index of refraction of the medium where the light propagates, and λ_0 is the central wavelength of the source. We can define the coherence envelope C_e of the interference pattern with the exponential function in the following equation:

$$C_e = \exp\left[-\left(\frac{\mathrm{OPD}}{lc}\right)^2\right]. \quad (3)$$

2.2 Working Principle of the Optical Phase Mask

The metrology instrument incorporates an innovative optical phase mask to perform dynamic white light interferometry without any moving part. Its working principle will be explained now before its implementation on the global optical layout of the instrument. Dynamic interferometry means acquiring all the data points needed to reconstruct each local interferogram on a single camera frame. The optical phase mask we conceive has a step design, where each step induces a change in OPD. Each step is made of the same material but has a different optical thickness. Considering two monochromatic light rays, Eq. (4) gives the OPD between the rays when one traverses a material with an optical thickness e, and the other propagates parallel on air. n is the material index of refraction at a specific wavelength

$$\mathrm{OPD} = e \cdot (n - 1). \quad (4)$$

According to Eq. (4), the change in OPD depends on the source's wavelength. In our case, we use a polychromatic source. Accordingly, the phase shift introduced by a step of the optical
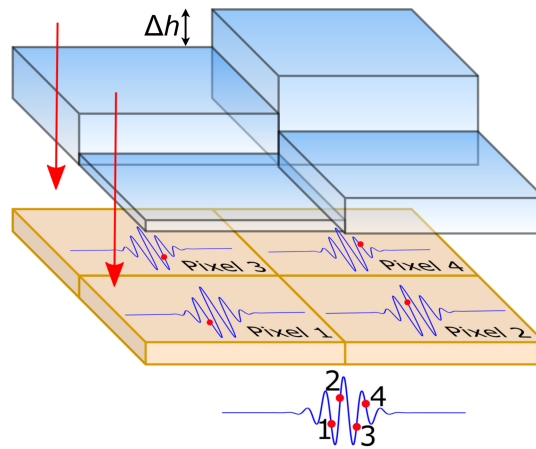
Fig. 1 A concept view of the optical phase mask designed to perform single-frame white light interferometry. Each step introduces a different OPD to the rays from the same local point. Accordingly, each step is associated with the measure at the detector of a different local white light interferogram sample point.

phase mask differs for the individual spectral constituents. This issue is also present in conventional scanning phase-shifting white light interferometers since the phase shift varies inversely with the wavelength. It should be noted that Hariharan proposed the principle of achromatic phase shifting for white light interferometry.[22] He used the Pancharatman phase, which is the phase shift produced by a cyclic change in the state of polarization of a light beam, and that is almost independent of the wavelength. The wavelength dependence of our optical phase mask introduces chromatic aberrations that limit the determination of the exact position of the mirror. Nevertheless, the chromatic aberrations of a phase shift lead to systematic measurement errors. Lehmann et al. proposed a method to correct these errors[23] numerically.

In addition to the optical phase mask, we add a microlenses array in front of the detector with a number of microlenses equivalent to the number of steps of the optical phase mask. The microlenses of the array are also square-shaped with identical dimensions to the steps of the phase mask. Accordingly, at the detector, we measure a sample point of the local white light interferogram for each pair of optical phase mask step and lens of the microlenses array. Then, we can reconstruct the full local white light interferogram with all the interferometer sample points of the field of view.

Figure 1 depicts a schematic representation of the optical phase mask working principle. We define the height difference, Δh, between consecutive steps using the following equation, Eq. (5). We obtain this equation through Eq. (4) to have a representative phase shift of $\pi/2$ or $\lambda/4$ between steps. The value $\pi/2$ is commonly used as the phase shift between consecutive data points on the previously referenced data processing methods of the white light interferograms. It is also a good compromise on the feasibility of constructing the optical phase mask according to the current machining techniques

$$\Delta h = \frac{\lambda}{8 \cdot (n-1)}, \tag{5}$$

where λ is the central peak wavelength of the source and n is the material index of refraction. As a reference, for an index of refraction of around 1.52, which corresponds to $N - BK7$ with a central wavelength at 500 nm, the height difference between consecutive steps is 120 nm. We expect a surface waviness of the phase mask lower than $\lambda/20$ for $\lambda = 633$ nm.

2.3 Optical Layout of the Instrument

Figure 2 depicts the schematic optical layout of the developed prototype, implemented on the basis of the Michelson two-arm interferometer. First, we collimate the light source after spatial filtering it. Then, we use a cube beam splitter (CBS) to split the incident light beam and recombine the beams reflected in the measurement and reference mirror. The reason to use a CBS is to avoid a compensation plate and, therefore, facilitate the alignment of the system when using a
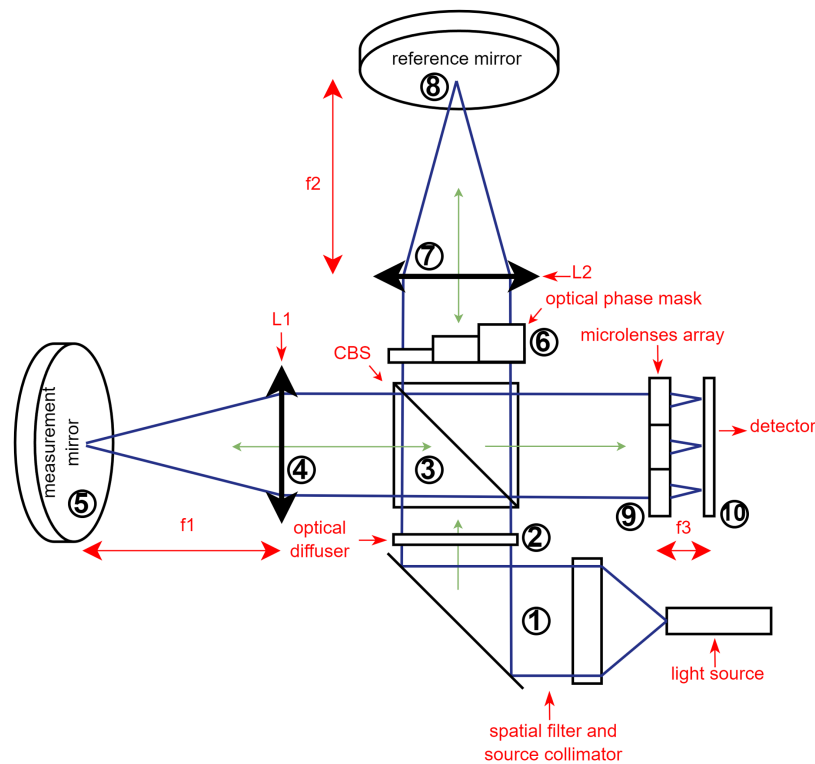
Fig. 2 A conceptual view of the metrology instrument we developed to characterize local changes in the topology of a mirror and local induced vibrations. To do this, the instrument measures a set of interference patterns of the same surface on the mirror at the detector on a single camera frame, each at a different OPD.

low-coherence source. We include an objective lens on the interferometer arms before the reference mirror and before the mirror to be characterized. In addition, the microlenses array we presented in Sec. 2.2 before the detector. Then, we locate the optical phase mask within the reference arm. We add a glass transparent diffuser from Edmund Optics before the CBS to have a uniform illumination of the optical field. Regarding the type of diffuser, we are limited by its rugosity properties since the diffuser scrambles the wavefronts and reduces the source's spatial coherence, which is already a limitation for us.

Figure 3 shows the experimental bench of the metrology instrument. It implements the optical layout presented in Fig. 2. We use a microlenses array of five-by-five microlenses. The optical phase mask has five by five steps. It is placed on the reference arm of the interferometer. The reference mirror (8) is mounted over a high-precision translation stage, LTS300C, from Thorlabs. We use the translation stage to adjust the OPD of the interferometer's two arms. It is instructive to note that the optical phase mask must be already on the reference arm during the alignment. This is because the thickness of the plate where the optical phase mask is engraved introduces a phase shift larger than the coherence length of the source, which will prevent the white light interferograms from forming. The height difference between the largest and the smallest step of the optical phase mask determines the maximum out-of-plane displacement of the measurement mirror that the instrument can measure. Accordingly, before using the instrument, we adjust the OPD to provide the highest contrast of the fringes in the middle range of the optical phase mask.

Figures 4(a) and 4(c) depict the microlenses array prototype and the optical phase mask prototype. Figures 4(b) and 4(d) are their respective computer-aided design (CAD) models. Both optical elements are engraved on a 9 mm by 9 mm MgF_2 subtract of 5 mm thickness. MgF_2 was proposed by the manufacturer as the material that best adapts to their engraving techniques. Besides, MgF_2 is vacuum-compatible. The microlenses array, Fig. 4(a), consists of five by five plano-convex square-shaped microlenses of 1.8 mm by 1.8 mm pitch. The focal length of
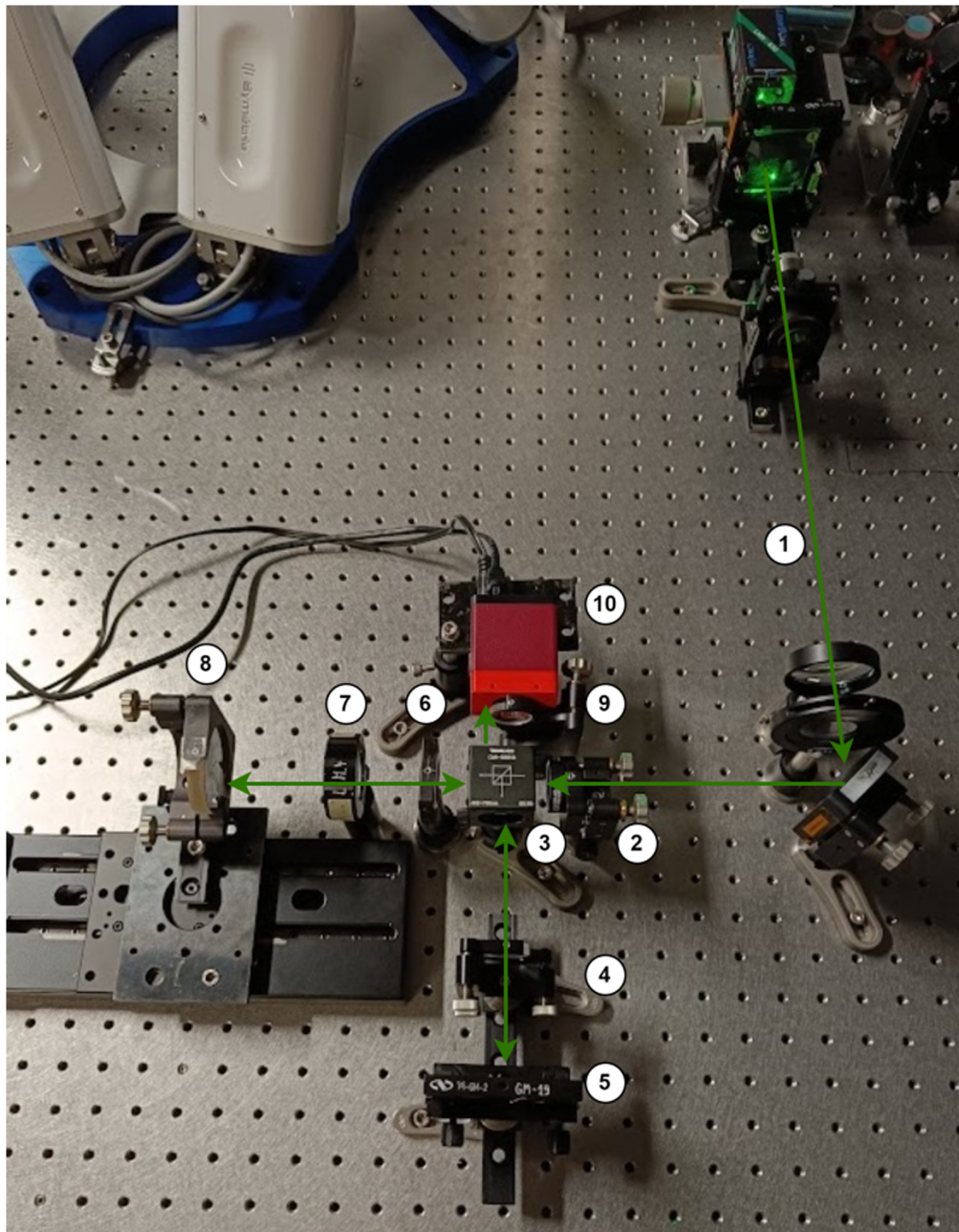
Fig. 3 Experimental setup to validate the measurement principle of the metrology instrument. (1) Spatial filtering and collimation of the source, (2) ground glass diffuser from Edmund Optics, (3) CBS 50/50, (4) lens L1, (5) measurement mirror, (6) optical phase mask, (7) lens L2, (8) reference mirror, (9) microlens array, and (10) Allied Vision Prosilica GE-2040 1.2" Monochrome CCD Camera modified with 3D printed components.

the microlenses is 10.4 mm. The optical phase mask consists of a grid of five by five steps of 1.8 mm by 1.8 mm and around 160 nm height difference between consecutive steps. Figure 4(b) shows an image of the optical phase mask obtained by back illuminating the mask. The optical phase mask required custom fabrication methods by the manufacturer, Wielandts UPMT in Belgium, to ensure the small height difference between steps. The base of the fabrication method was the freeform diamond turning technique. In this technique, a cutting tool is pressed against the rotating workpiece to cut and remove material. For the optical phase mask, the center of the mask was aligned with the spindle axis, and the cutting tool spiraled inward from one surface of the mask to the other as it rotated. One key parameter was the parallelism between the front and
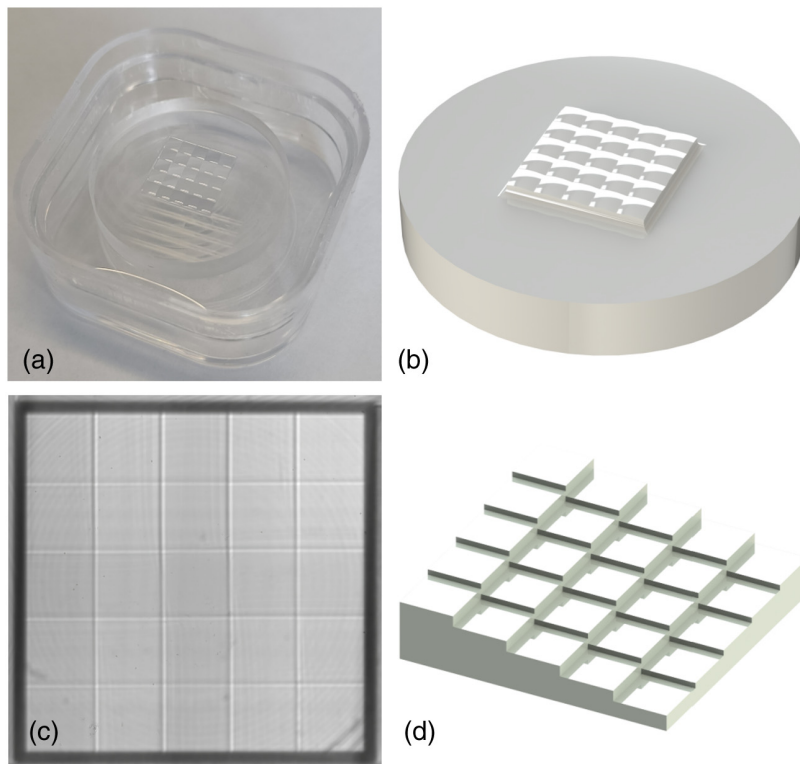
Fig. 4 (a) Microlenses array used in the prototype of the white light interferometer. The array contains 25 plano-convex microlenses of 1.8 mm by 1.8 mm pitch each. (b) CAD design of the microlenses array. (c) Manufactured optical phase mask of 25 steps and 160 nm height difference between consecutive steps. (d) CAD design of the optical phase mask where the height difference has been exaggerated for visualization purposes.

rear surfaces of the optical phase mask to reduce the internal reflections as much as possible. Their fabrication method ensured a maximum parallelism deviation of 1 μm on a piece of 5 mm thickness. Therefore, with the 25 steps of the optical phase mask, we can obtain 25 interference patterns of the same surface we characterize on the mirror. The mirror's surface, characterized by the experimental instrument, is about 1 cm in diameter. The range between the smallest and the largest step of the optical phase mask is approximately 4 μm.

2.4 Measurement of Local Induced Vibrations

One of the applications of our instrument is to measure the local induced vibrations of a suspended mirror. We characterize low-frequency out-of-plane induced vibrations ranging between 0.1 and 10 Hz. For this characterization, we use the pair of local white light interferograms obtained in two consecutive camera frames, and that correspond to the same local point on the mirror. First, we precisely determine the peak of the coherence envelope of each interferogram with a Hilbert transform or a mathematical function that adapts to the data points (see Sec. 2.6).

Then, we measure the variation of the position of the two peaks identified due to local vibration. This difference in position should be zero in an ideal case when the mirror is perfectly isolated from vibrations. We illustrate the procedure in Fig. 5. In this figure, we normalize the optical intensity of the interference pattern data points to a value between −1 and 1, but the optical intensity values are always positive. Then, we can repeat the procedure with all the local points within the mirror surface we characterize.

Measuring local induced vibrations at low frequencies is one of the most significant advantages of our proposed instrument. The total height difference between the smallest and the largest step of the optical phase mask determines the maximum amplitude of mirror displacement between two consecutive camera frames we can measure.
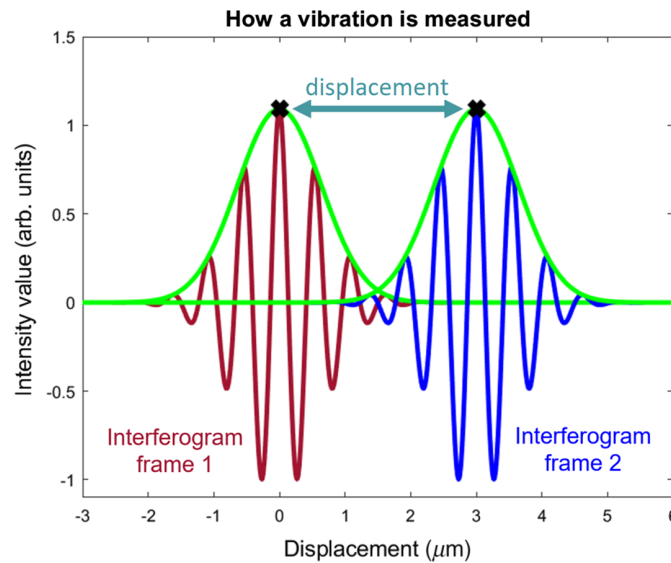
Fig. 5 By measuring the displacement of the interference pattern between two consecutive camera frames, we can calculate the amplitude of the local vibration.

2.5 Measurement of Local Topology Changes

The second application of the metrology instrument is the measurement of local changes in the topology of the mirror. In Fig. 6, we depict the computer simulation of the measurement principle with a two-by-two-step optical phase mask. Figure 6(a) represents a CAD of the measurement mirror (5) of Fig. 2. The mirror is fixed within the suspended cage inside the vacuum chamber and cooled down at cryogenic temperatures. The mirror of the figure depicts an exaggerated scale of a mirror deformation in the surface for illustration purposes. Figure 6(b) shows an example of the four interference patterns of the mirror deformation that is obtained with an optical phase mask of two by two steps. Each interference pattern characterizes the same mirror surface, but each interference pattern has a different OPD. This simulation was realized with a source of spectral range from 400 to 600 nm and a central wavelength at 550 nm. Figure 6(c) illustrates the reconstruction of the white light interferogram for a selected local point of the mirror surface under characterization, represented by a yellow square in Fig. 6(a). The data points 1 to 4 correspond to points 1 to 4 of Fig. 6(b). The detection of the coherence peak of the white light interferogram, again with a Hilbert transform or a mathematical function on the data points, allows us to determine the topology of the mirror for this specific local point of the surface. The instrument's lateral resolution, defined as the smallest distance between two surface features in the x-y plane of the mirror for which the features are clearly distinguishable,[24] is a relevant parameter for the interferometer. The focal length of the microlenses, which is the smallest optical component, the pixel pitch and the object distance limit the lateral resolution on the object plane. In our optical experiment, for an object distance between 250 and 150 mm, the lateral resolution in the object plane is approximately between 0.2 and 0.1 mm, respectively. The lateral resolution in the image plane will be camera-limited. This limitation is because the diffraction-limit value given by the Rayleigh criterion for the microlens's optical parameters is smaller than the pixel pitch of the detector, which is 7.5 μm. Figure 6(d) represents the full reconstruction of the mirror topology obtained by applying the interferogram analysis method of (b) and (c) to all the local points. On a single camera frame, a full reconstruction of the mirror surface is obtained, enabling real-time monitoring of the mirror topology, which can be affected by thermo-mechanical fluctuations.

2.6 Determination of the Coherence Envelope Maximum

The technique aims to evaluate local topology changes and induced vibrations by finding the maximum of the coherence envelope of the interference pattern. Various methods are available to estimate its position according to the bibliography.[11]
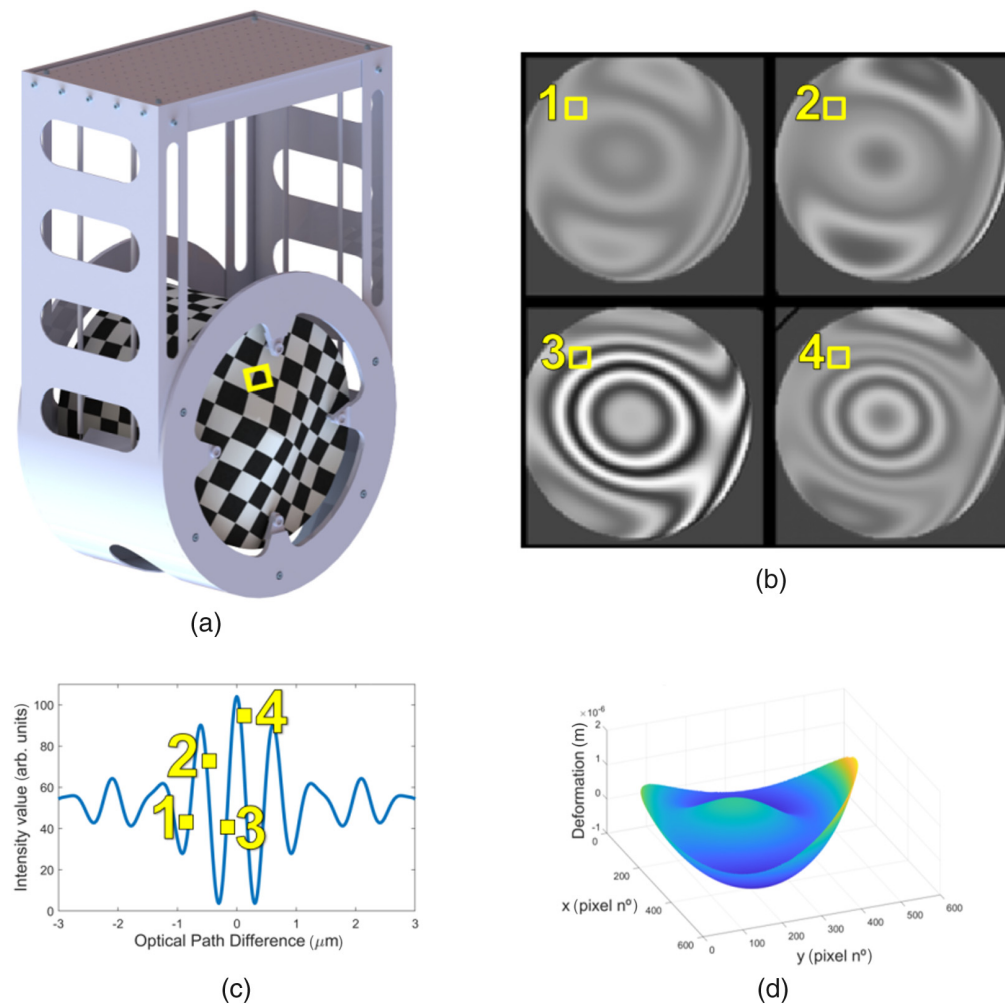
Fig. 6 Numerical simulation of the instrument measurement principle to illustrate the process of characterizing the mirror surface topography. (a) CAD of the mirror under characterization fixed within its attachment cage. The deformation of the mirror surface has been exaggerated for illustration purposes. The yellow square of (a) represents a local point of the mirror surface. (b) The four interference patterns for an optical phase mask of four steps simulated with the ray tracing software ASAP NextGen. The local point of (a) is located at each interference pattern with yellow squares and the numbers 1 to 4. (c) Reconstruction of the local low-coherence interferogram with the data points 1 to 4 of the four interference patterns of (b). The maximum of the interferogram's coherence envelope determines the local point's topology. d) Example of the mirror's full topology acquired by applying the process depicted from (a) to (c) to all the local points inside the surface characterized in the mirror. Panel (d) is obtained on a single camera frame.

The centroid method, based on determining the center of gravity of the interference pattern over the OPD, and the frequency-domain analysis methods require more than sixty sample points.[2,11] Consecutive camera frames capture sample point along the interferogram. Between frames, the reference mirror is displaced, changing OPD. In our case, we take measurements of the interference pattern at each step of the optical phase mask. The height difference between the steps of the optical phase mask provides the OPD separation between the measurement points. Currently, we have a limit on the maximum number of steps due to the ongoing development of the technology required for manufacturing the mask. As a result, we prioritize interferogram analysis methods that require a minimal number of samples for pattern reconstruction and detecting the coherence envelope peak.

A commonly used method in long-coherence interferometry is PSI, which requires a low number of sample points, usually less than 10.[11,25] The PSI method calculates the difference in path length between the two arms of the interferometer by using the phase value of the
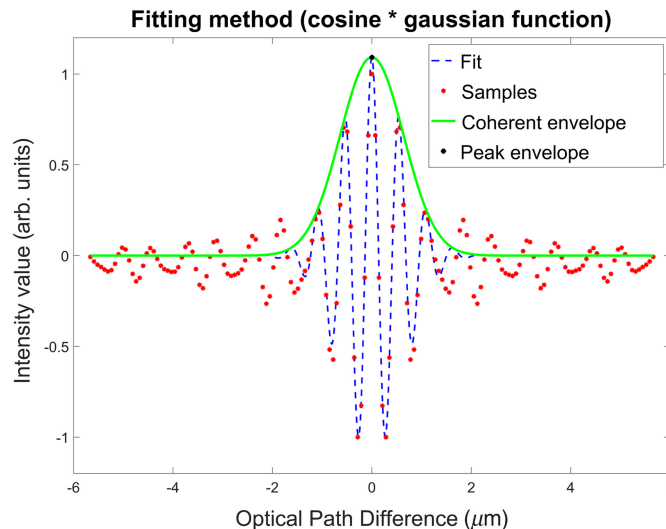
Fig. 7 Determination of the peak of the coherence envelope by fitting a mathematical function to the samples. We obtain each sample with a different step of the optical phase mask.

interference wave. To determine the wave phase, PSI employs the intensity values of the interferograms captured by the detector over a sequence of consecutive camera frames. Once again, the reference mirror is moved using a translation stage between camera frames. To use the PSI equations, a specific phase shift between camera frames is required. However, in our case, we do not use a translation stage. Instead, we use an optical phase mask that introduces a phase shift by steps of different optical thicknesses. The phase shift depends on the material index of refraction, which in turn depends on the wavelength.

Our current methods are designed to work seamlessly with the phase mask we developed. One of the techniques we use involves determining the peak of the coherence envelope through a Hilbert transform. Additionally, we have defined a function based on the product of a cosine and a Gaussian function to fit the intensity points and locate the maximum of the envelope. We have illustrated this method in Fig. 7, where we have normalized the intensity from −1 to 1, taking into account that the intensity value is always positive. Our ultimate goal is to be able to reconstruct the interferogram even in the presence of a faulty sample, unwanted signal noise, or uneven phase shifts between samples. Hence, the higher the amount of steps in the optical phase mask, the more optimal it is. Another reason for many steps is directly related to the project of a gravitational wave observatory where we implement the metrology instrument. As the introduction mentions, an innovative hanging module suspends the mirror inside the vacuum chamber. During the initial operation of the metrology instrument, there will be an unknown on the relative distance between the instrument and the hanging mirror to be characterized. To calibrate the instrument, we must determine the distance between the instrument and the observed region. By consequence, light source's coherence region falls within the phase mask's boundaries. To achieve the objective, an optical phase mask with multiple steps must be used.

3 Experimental Results

We built the experimental setup of Fig. 3 to prove the instrument's theoretical working principle. At the first stage of development, the proposed instrument was investigated only with the microlenses array. The aim was to obtain a repetition of the interference pattern on the mirror under characterization. As explained in previous sections, we need to obtain one interference pattern for each microlens of the microlenses array. The experimental bench was tested with three different light sources: a laser source from Oxxius at 532 nm peak wavelength and two low-coherence sources, including an LED with a 60 nm FWHM at 532 nm peak wavelength from Thorlabs, as well as the halogen white light source, Ocean Insight HL 2000-FHSA-LL. We obtained interference fringes with all three sources under test. Regarding fringe visibility and contrast, the best interference patterns were acquired with the Oxxius source, the source with the longest

coherence. In the case of low-coherence sources, the maximum contrast that can be successfully attained in a single image is determined by the camera's dynamic range. The dynamic range characterizes the ability of a camera system to measure and distinguish different levels of light. Figure 8 depicts the experimental results obtained at the detector on a single camera frame after the alignment of the optical setup. It represents a repetition of the interference pattern of the surface characterized in the mirror.

In our work, we used the contrast and visibility of the interference fringes as the figures of merit to do a qualitative evaluation of the alignment of the optical setup. Figure 3 illustrates the optical setup that maximizes fringe contrast and ensures the visibility of the repetition of the interference pattern for each microlens. Figure 9 shows the results for four configurations of the optical setup to explain how the optical components and their position affect the contrast and visibility of the fringes.

4 Discussion

Our laboratory's optical experiment aims to validate our proposed white light interferometry approach using a microlens array and a phase mask which leads to obtaining a replication of the interference pattern of the surface seen on the mirror multiple times within a single camera frame.

To align the optical system, we captured interference fringes with a camera to detect the highest contrast. The position of the optical components associated with the highest contrast corresponds to the optimal alignment configuration. After aligning the system by ensuring equal arm lengths for the interferometer, we achieved the desired repetition of the interference pattern shown in Fig. 8 by integrating the microlens array in the optical setup. Each microlens corresponds to one interference pattern. The interference patterns form a regular grid with nearly equidistant centers. Two factors affecting the apparent offset were observed during measurements. First, there is a misalignment between the optical axes of the microlenses and lenses L1 and L2. Second, the diffuser in the optical setup causes light divergence, which is more noticeable. Additionally, the interference fringes exhibit a combined coma and astigmatism aberration, as reported in Ref. 25.
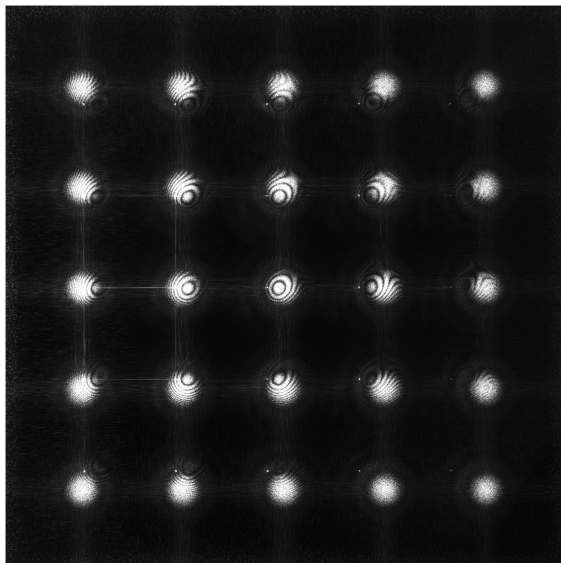

Fig. 8 Single-frame captured using the optical setup of Fig. 3 including the microlenses array only. A repetition of the interference pattern is obtained. Each interference pattern is associated with one microlens. The centers of the interference patterns are equidistant to their neighbor. The apparent offset in their positions is a result of the light divergence caused by the diffuser in the optical setup and the misalignment of the microlens' optical axes.

Figure 9 shows four variations of the same optical setup, compared in terms of optical contrast and visibility of interference fringes. In Fig. 9(a), we defocused the microlenses array to demonstrate that the repetition of the interference pattern is no longer visible. On the other hand, according to Fig. 9(b), a low contrast interference pattern is observed when the microlenses array is removed. Conversely, in Fig. 9(c), a high-contrast interference pattern is acquired by removing the diffuser and defocusing the microlenses array. However, the interference pattern is no longer repeated for each microlens. Instead, each microlens captures a portion of the interference pattern that is obtained when the microlens array is removed from the optical layout and images it onto the detector. By rotating each image 180 deg, a similar pattern to Fig. 9(d) is obtained. Figure 9(d) was captured without the diffuser and microlenses array.

One of the limits of the interferometer is the maximum spot diameter to be analyzed on the mirror. Large-diameter white light beams are very sensitive to misalignment errors. It introduces phase differences across the beam, which reduces the beam's coherence and makes it challenging to obtain useful interferograms. On the other hand, there are potential sources of errors that we must take into account for the correctness of the measurements. One error source is the internal reflections on the optical phase mask. To reduce them, we may modify the layout of the interferometer arms so that the beam of light passes only one time through the optical phase mask. Another potential solution is to use an antireflective coating on a new iteration of the optical phase mask. Then, to avoid aliasing and unwanted stray light between consecutive steps of the optical phase mask, we consider adding a grid of apertures in front of the mask.
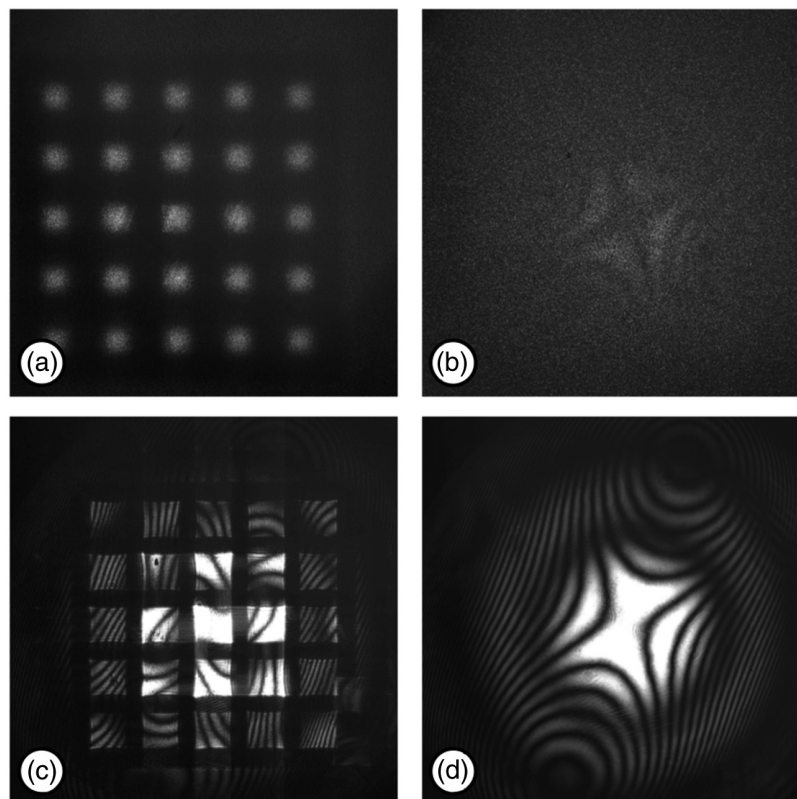

Fig. 9 Experimental results for four relevant variants of the optical setup of Fig. 3. (a) Defocusing the microlenses array renders the interference fringes no longer visible at the detector. (b) Removing the microlenses array from the optical layout results in low-contrast fringes at the detector plane. (c) Without the optical diffuser and with a defocused microlenses array, we obtain the highest contrast interference fringes among all the optical setups but not the repetition of the interference pattern for each microlens. (d) In the absence of the diffuser and the microlenses array in the optical layout, a high-contrast interference pattern emerges at the detector plane.

5 Conclusion

The capability to simultaneously measure local topology changes and induced vibrations of optical components represents a significant advancement in optical metrology. This paper introduced a metrology instrument capable of implementing this innovative measurement principle.

The proposed interferometer concept includes an optical phase mask and a microlenses array to do real-time monitoring of the mirror surface topology without mechanical scanning components that may cause unwanted additional vibrations. In this paper, we have shown numerically the working principle of the metrology instrument. Then, we presented the stage of development of a proof of concept of the interferometer. The working principle of the microlenses array has been demonstrated experimentally.

We developed the metrology instrument on the frame of the ET project to measure the induced vibrations and topology change of a cryogenic mirror suspended inside a vacuum chamber. However, it is of extensive usability in other diverse applications related to real-time measurement of various fast physical processes and real-time characterization of optical components with all the advantages of low-coherence interferometry.

As for future work, we aim to enhance the contrast of the interference fringes and the instrument resolution.

References

1. J. C. Wyant, "White light interferometry," *Proc. SPIE* **4737**, 98–107 (2002).
2. P. Sandoz, R. Devillers, and A. Plata, "Unambiguous profilometry by fringe-order identification in white-light phase-shifting interferometry," *J. Mod. Opt.* **44**, 519–534 (1997).
3. P. De Groot and L. Deck, "Surface profiling by analysis of white-light interferograms in the spatial frequency domain," *J. Mod. Opt.* **42**(2), 389–401 (1995).
4. Y. Deng and D. Chu, "Coherence properties of different light sources and their effect on the image sharpness and speckle of holographic displays," *Sci. Rep.* **7**, 5893 (2017).
5. P. De Groot, "Stroboscopic white-light interference microscopy," *Appl. Opt.* **45**, 5840–5844 (2006).
6. M. Takeda, "Optical metrology: methodological analogy and duality revisited," *Proc. SPIE* **11813**, 118130J (2021).
7. J. E. Millerd and M. North-Morris, "Dynamic interferometry: measurement of space optics and structures," *Proc. SPIE* **10329**, 103291G (2017).
8. O. Y. Kwon, "10.6 micron interferometry and beyond," *Proc. SPIE* **11813**, 118130F (2021).
9. P. Pavliček and E. Mikeska, "White-light interferometer without mechanical scanning," *Opt. Lasers Eng.* **124**, 105800 (2020).
10. Y. Ferrec et al., "Nanocarb part 1: compact snapshot imaging interferometer for co2 monitoring from space," *Proc. SPIE* **11180**, 1118021 (2019).
11. P. De Groot, "Principles of interference microscopy for the measurement of surface topography," *Adv. Opt. Photonics* **7**, 1–65 (2015).
12. J. Woo Jeon et al., "High-speed polarized low coherence scanning interferometry based on spatial phase shifting," *Appl. Opt.* **58**(20), 5360–5365 (2019).
13. A. Sider et al., "E-test: a compact low-frequency isolator for a large cryogenic mirror," *Classical Quantum Gravity* **40**, 165002 (2023).
14. A. Sider et al., "E-test prototype design report," tech. rep. (2022).

15. J. Vilaboa Pérez et al., "Low coherence interferometry to characterize the induced vibrations and topology change of the cryogenic mirror of the Einstein Telescope prototype," *Proc. SPIE* **12188**, 121881E (2022).
16. J. Vilaboa Pérez et al., "Experimental results of an innovative dynamic low-coherent interferometer for characterizing a gravitational wave detector," *Proc. SPIE* **12672**, 126720F (2023).
17. H. Kaneda et al., "Cryogenic optical testing of SIC mirrors for ASTRO-F and C/SIC composite mirrors for SPICA," in *Eur. Space Agency, (Spec. Publ.) ESA SP (554)*, pp. 699–706 (2004).
18. B. Saif, L. Feinberg, and R. Keski-Kuha, "High-speed interferometry for James Webb Space Telescope testing," *Proc. SPIE* **11813**, 118130U (2021).
19. D. Malacara and Optical Shop Testing, 3rd ed., Wiley-Interscience (2006).
20. J. H. Kim, "High precision signal processing algorithm for white light interferometry," *Sensors* **8**(12), 7609–7635 (2008).
21. P. Lehmann, "Aspect ratio of elongated polychromatic far-field speckles of continuous and discrete spectral distribution with respect to surface roughness characterization," *Appl. Opt.* **41**(10), 2008–2014 (2002).
22. P. Hariharan, "Achromatic phase-shifting for white-light interferometry," *Appl. Opt.* **35**(34), 6823–6824 (1996).
23. P. Lehmann, P. Kühnhold, and W. Xie, "Reduction of chromatic aberration influences in vertical scanning white-light interferometry," *Meas. Sci. Technol.* **25**(6), 065203 (2014).
24. "Geometrical Product Specifications (GPS)-Surface Texture: Areal-Part 600: Metrological Characteristics for Areal-Topography Measuring Methods," Standard ISO DIS 25178-600:2019, International Organization for Standardization, Geneva, CH (2019).
25. E. P. Goodwin and J. C. Wyant, *Field Guide to Interferometric Optical Testing*, 1st ed., SPIE-The International Society for Optical Engineering (2006).

Jesús Vilaboa Pérez PhD candidate in optical engineering at the Space Center of Liège, Belgium. He received his BSc degree in aerospace engineering from the University of León, Spain and his MSc degree in aerospace engineering, with a specialization in space engineering from the University of Liège, Belgium. His main work is on the E-TEST project. E-TEST is a technology demonstrator for the future Einstein Telescope dedicated to measuring and characterizing gravitational waves.

Marc Georges is the head of Optics Laboratory and coordinator of Academic and Scientific Affairs at the Space Center of Liège. He is an SPIE Fellow Member. He received his PhD in dynamic holographic interferometry from the University of Liège.

Juriy Hastanin is the expert physicist at the Surface Engineering Laboratory of the Space Center of Liège. He received his PhD in surface plasmon resonance technology from the University of Liège.

Jérôme Loicq is a professor in space instrumentation at the Technical University of Delft, Netherlands and the University of Liège. He received his PhD in material sciences (nanotechnology), optoelectronics, and non-linear optics from the University of Liège.